Copy 42
RM SL56E15

[redacted]

RESEARCH MEMORANDUM

for the

Bureau of Aeronautics, Department of the Navy

SOME TRANSONIC AERODYNAMIC CHARACTERISTICS OF A MODEL SIMILAR TO THE McDONNELL F3H-2N AIRPLANE

TED NO. NACA DE 351

By Norman L. Crabill and Bruce G. Jackson

Langley Aeronautical Laboratory
Langley Field, Va.

UNCLASSIFIED; EFFECTIVE 4-29-65
AUTHORITY F. J. DROBKA (ATSS-A)
memo dated 5-13-65

DECLASSIFIED BY AUTHORITY OF NASA
CLASSFICATION CHANGE NOTICES NO. 19
DATED 5-26-65 ITEM NO. 14

[redacted]

NATIONAL ADVISORY COMMITTEE
FOR AERONAUTICS

WASHINGTON

NATIONAL ADVISORY COMMITTEE FOR AERONAUTICS

RESEARCH MEMORANDUM

for the

Bureau of Aeronautics, Department of the Navy

SOME TRANSONIC AERODYNAMIC CHARACTERISTICS OF A MODEL SIMILAR TO THE McDONNELL F3H-2N AIRPLANE

TED NO. NACA DE 351

By Norman L. Crabill and Bruce G. Jackson

SUMMARY

A model similar to the McDonnell F3H-2N airplane has been tested at transonic speeds by the National Advisory Committee for Aeronautics with the free-flight technique to determine its pitch-up and buffet boundaries in addition to the longitudinal stability and control data obtainable with the pulse-tail technique. Examination of the data revealed that at transonic speeds the stability is less at low trim angles of attack than at high trim angles of attack up to a limit. Beyond this limiting angle, the stability was reduced and became zero at angles of attack varying from 13° at $M = 0.7$ to 9° at $M = 0.9$. It was not possible to determine the buffet boundary.

INTRODUCTION

At the request of the Bureau of Aeronautics, Department of the Navy, the National Advisory Committee for Aeronautics has tested a model similar to the McDonnell F3H-2N airplane by the free-flight technique to determine its pitch-up and maneuver buffet boundaries in addition to the longitudinal stability and control data obtainable with the pulse-tail technique. Previous free-flight tests of models of the McDonnell XF3H-1 and F3H-1N configurations are reported in references 1, 2, and 3. Results of the present test are presented herein with no detailed analysis in order to expedite publication. The model was supplied by the McDonnell Aircraft

[redacted]

Corporation and the test was made at the Pilotless Aircraft Research Station at Wallops Island, Va.

SYMBOLS

Positive directions of forces, moments, and displacements are indicated in figure 1.

A_L acceleration parallel to fuselage center line, g units

A_N acceleration perpendicular to fuselage center line, g units

A_T acceleration perpendicular to plane of symmetry, g units

$\bar{c}$ wing mean aerodynamic chord, ft

C_{BM} wing bending-moment coefficient, $\dfrac{\text{Aerodynamic bending moment}}{q\frac{S}{2}\frac{b}{2}}$, about 23.4 percent at spanwise station

C_c chord force coefficient, $-A_{L_{cg}}\dfrac{W}{qS}$

C_D drag coefficient, $C_N \sin\alpha + C_c \cos\alpha$

C_L lift coefficient, $C_N \cos\alpha - C_c \sin\alpha$

$$\frac{\Delta C_L}{\Delta C_{L_{max}}} = \frac{\text{Value of } C_L \text{ on oscillation envelope} - C_{L_t}}{\text{Max value of } C_L \text{ on oscillation envelope} - C_{L_t}}$$

C_m pitching-moment coefficient about center of gravity,

$$\frac{I_Y \frac{g}{l}\left(A_{N_N} - A_{N_{cg}}\right)}{qS\bar{c}}$$

$C_{m_q} + C_{m_{\dot{\alpha}}}$ dynamic-longitudinal-stability parameter, radian measure

C_N normal-force coefficient, $A_{N_{cg}}\dfrac{W}{qS}$

C_Y lateral-force coefficient, $A_T\dfrac{W}{qS}$

[redacted]

g — acceleration due to gravity, ft/sec^2

I_X — mass moment of inertia of model in roll, slug-ft^2

I_Y — mass moment of inertia of model in pitch, slug-ft^2

I_Z — mass moment of inertia of model in yaw, slug-ft^2

l — longitudinal distance between normal accelerometers

L/D — lift-drag ratio

M — free-stream Mach number

Δp_{wing} — pressure measured on upper surface of right wing minus free-stream static pressure, lb/sq ft

P — period of longitudinal motion, sec

p_∞ — free-stream static pressure, lb/sq ft

q — free-stream dynamic pressure, $0.7p_\infty M^2$

RN — Reynolds number based on $\bar{c}$

^oR — free-stream static temperature, deg Rankine

S — model wing area, sq ft

T — elapsed time after take off, sec

$T_{1/2}$ — time for amplitude of longitudinal motion to damp to half amplitude, sec

V — free-stream velocity, ft/sec

V_w — wind velocity, ft/sec

W — weight of model, lb

x_{ac} — aerodynamic-center location, distance aft leading edge of mean aerodynamic chord, ft

α — angle of attack of fuselage reference at center of gravity, deg

$$\frac{\Delta\alpha}{\Delta\alpha_{max}} = \frac{\text{Value of } \alpha \text{ on oscillation envelope} - \alpha_t}{\text{Max value of } \alpha \text{ on oscillation envelope} - \alpha_t}$$

γ flight-path angle, deg

θ angle of fuselage center line relative to fixed reference, deg

δ deflection of horizontal stabilizer relative to fuselage reference, deg

ψ_w direction from which wind is blowing, degrees from true north

Subscripts:

av average

cg center of gravity

max maximum

o value at minimum drag

N nose

t trim

Derivatives with respect to a quantity are indicated as shown in the following example:

$$C_{m_\alpha} = \frac{dC_m}{d\alpha}$$

Specific conditions for which a quantity is evaluated are indicated as shown in the following example:

$$C_{m_{\alpha=0}} = \text{Pitching-moment coefficient at } \alpha = 0$$

DESCRIPTION OF MODEL AND INSTRUMENTATION

Model

The model, described in figures 2(a), (b), (c), and (d) and table I, was originally constructed as a 1/10-scale model of the McDonnell XF3H-1 airplane. Subsequently, a McDonnell F3H-2N wing was substituted, and the XF3H-1 horizontal tail was relocated to the more aft position of the F3H-2N horizontal-tail position. The actual F3H-2N fuselage is somewhat fatter, and the horizontal tail is somewhat larger. This model is similar in construction and instrumentation to the model described in reference 3. An electrohydraulic system pulsed the entire horizontal stabilizer abruptly between stops of about $+1^{\circ}$ and -6° relative to the fuselage center line. There was no air flow through the model, since the ducts were blocked just inside the inlets.

Instrumentation

The model was instrumented so that Mach number, angle of attack, lift, drag, and pitching moment could be determined at every instant. In addition, measurements of wing-root bending moment and absolute pressure on the upper surface of the right wing (figs. 2(a) and (d)) were made to aid in determining the buffet boundary. These data were transmitted from the model by an NACA telemeter. Altitude of the model and meteorological conditions were determined from ground-based-radar and rawinsonde measurements.

TESTS AND METHODS OF ANALYSIS

The model was tested by the free-flight rocket-boosted-model technique described in reference 4. Axes systems used in the reduction and analysis of the data are shown in figure 1. A time history of some of the more important quantities obtained as the model decelerated from $M = 1.28$ to 0.69 is given as figure 3. The test conditions are summarized in figure 4.

RESULTS AND DISCUSSION

The results of the test are given in figures 5 through 20. In order to expedite publication of these data, no detailed analysis will be made. However, several simple observations are worth noting.

Trim

In figure 5, the trim lift coefficient and angle of attack for $\delta \approx -6^{\circ}$ show abrupt variations with Mach number near $M = 0.9$.

Lift

In figures 6 and 7, it is seen that the lift-curve slope increases with angle of attack. Also, near $M = 0.7$ to 0.8, $C_{L_{max}}$ depends significantly on the sign of $\dot{\alpha}$, figure 7(c).

Drag

The drag data, figures 8, 9, 10, include base drag and, since the model inlets were blocked off, an additive drag due to duct spillage. Minimum drag, figure 10(a), seems to be affected somewhat by stabilizer position. Since the XF3H-1 fuselage used on this model is somewhat more slender than the actual F3H-2N fuselage, the minimum drag and $(L/D)_{max}$ data obtained in this test can not be applied directly to the F3H-2N airplane.

Dynamic Stability

The values of $C_{m_q} + C_{m_{\dot{\alpha}}}$ presented in figure 11(c) were determined for the low α range, except for the point at $M = 1.1$ which is for the high α range. (These α ranges are defined in fig. 13(b).) The dashed portion of the curve is less accurately defined than the solid part.

Static Pitching Moment

Static stability.- By plotting C_m against α, figure 12, the static-stability derivative C_{m_α} was obtained as a function of α (figs. 13(a) and (b)). The aerodynamic-center location (figs. 13(c) and (d)) was obtained from plots of C_m against C_L, although these plots are not presented. The results show (fig. 13) that at all Mach numbers of the test, the stability is less at low α_t ($\delta \approx +1^\circ$) than at high α_t ($\delta \approx -6^\circ$) up to a certain limit of angle of attack. Beyond this limiting angle, the stability is reduced and becomes zero at angles of attack varying from 13° at $M = 0.7$ to 9° at $M = 0.9$. The pitching-moment coefficients at zero angle of attack and at zero lift, given in figure 14 for the two stabilizer settings, exhibit no abrupt variations with Mach number. Again, caution must be used in applying these results to the F3H-2N airplane because of the smaller horizontal tail used on the test model.

Control effectiveness.- The effects of horizontal-stabilizer deflection on lift, drag, and static-pitching-moment coefficients (fig. 15) are also not directly applicable to the F3H-2N airplane.

Aerodynamic Wing Bending Moment

As for the other quantities, this aerodynamic wing bending moment is also markedly nonlinear with angle of attack (figs. 16 and 17) indicating that most of the nonlinearities in total airplane forces and moments can probably be traced to the direct contribution of the wing. Since the lift on the portion of the wing outboard of the strain gage was not measured separately, these data cannot be used to determine the lateral center of pressure.

Wing Pressure Coefficient

The jump in $\frac{\Delta p_{wing}}{q}$ when plotted against α (figs. 18 and 19) is probably caused by the passage of a shock over the orifice location. Note that at $M = 0.95$ (fig. 19(b)) this break occurs at $\alpha = -1.8^{\circ}$ $\left(\alpha_{wing} \approx 0^{\circ}\right)$.

Buffet

The telemeter records were inspected in order to determine the conditions under which buffet oscillations appeared. The results, plotted in figures 20(a) and (b), were inconclusive; a spread of about 8° in angle of attack at $M = 0.7$ and of 3° at $M = 0.9$ is shown in figure 20(b).

CONCLUDING REMARKS

A model resembling the McDonnell F3H-2N airplane was tested at transonic speeds by the free-flight technique primarily to determine its pitch-up and buffet boundaries. Examination of the data revealed that:

1. At transonic speeds the stability is less at low trim angles of attack than at high trim angles of attack up to a certain limit. Beyond

this limiting angle, the stability was reduced and became zero at angles of attack varying from 13° at $M = 0.7$ to 9° at $M = 0.9$.

2. It was not possible to determine the buffet boundary.

Langley Aeronautical Laboratory,
National Advisory Committee for Aeronautics,
Langley Field, Va., April 30, 1956.

Norman L. Crabill

Norman L. Crabill
Aeronautical Research Scientist

Bruce G. Jackson

Bruce G. Jackson
Aeronautical Research Scientist

Approved: Joseph A. Shortal

Joseph A. Shortal
Chief of Pilotless Aircraft Research Division

mfh

REFERENCES

1. Crabill, Norman L.: The Effects of Extensible Rocket Racks on Lift, Drag, and Stability of a 1/10-Scale Rocket-Boosted Model of the McDonnell XF3H-1 Airplane for a Mach Number Range of 0.60 to 1.34 - TED No. NACA DE 31. NACA RM SL53F15, Bur. Aero., 1953.

2. Crabill, Norman L., and McFall, John C., Jr.: Summary of the Lift, Drag, and Stability of 1/10-Scale Rocket-Boosted Models of the McDonnell XF3H-1 Airplane for a Mach Number Range of 0.6 to 1.4 As Affected by the Operation of Extensible Rocket Racks - TED No. NACA DE 351. NACA RM SL54A18, Bur. Aero., 1954.

3. Crabill, Norman L.: Lift, Drag, Static Stability, and Buffet Boundaries of a Model of the McDonnell F3H-1N Airplane at Mach Numbers From 0.40 to 1.27 - TED No. NACA DE 351. NACA RM SL56A13, Bur Aero, 1956.

4. Gillis, Clarence L., Peck, Robert F., and Vitale, A. James: Preliminary Results From a Free-Flight Investigation at Transonic and Supersonic Speeds of the Longitudinal Stability and Control Characteristics of an Airplane Configuration With a Thin Straight Wing of Aspect Ratio 3. NACA RM L9K25a, 1950.

130

TABLE I

PHYSICAL CHARACTERISTICS OF THE TEST MODEL

(a) Mass characteristics

Center-of-gravity location:	
Longitudinal, percent M.A.C.	27.9
Vertical, in. above fuselage reference	0.26
Weight, lb	139.7
Wing loading, lb/sq ft	26.9
Moments of inertia:	
I_X, slug-ft^2	1.006
I_Y, slug-ft^2	7.297
I_Z, slug-ft^2	7.832

(b) Geometrical characteristics

	Wing	Stabilizer	Fin
Aspect ratio	2.41	3.00	1.118
Sweepback of quarter-chord line, deg	43.0	45.0	45.0
Taper ratio	0.412	0.50	0.50
Incidence, deg	1.8	+1 and -6	0
Dihedral	0	0	0
Area (total), sq ft	5.19	0.70	0.455
Span, in.	42.40	17.40	8.55
Root chord (theoretical), in.	25.00	7.72	10.200
Tip chord (theoretical), in.	10.30	3.86	5.100
Mean aerodynamic chord, in.	18.67	6.004	7.933
Fuselage station of vertex, in.	18.00	57.94	54.730
Fuselage station of L.E. of M.A.C., in.	28.134	62.24	59.10
Spanwise station of M.A.C., in.	9.122	3.867	
Airfoil section at root	t/c = 0.0677; max. camber, 0.0095 at 11.2 percent c	NACA 0007-1.16 38/1.14	NACA 0007-1.16 38/1.14 mod.
Airfoil section at tip	t/c = 0.0639; max. camber, 0.0159 at 27.2 percent c	NACA 0007-1.16 38/1.14	NACA 0007-1.16 38/1.14 mod.

[redacted]

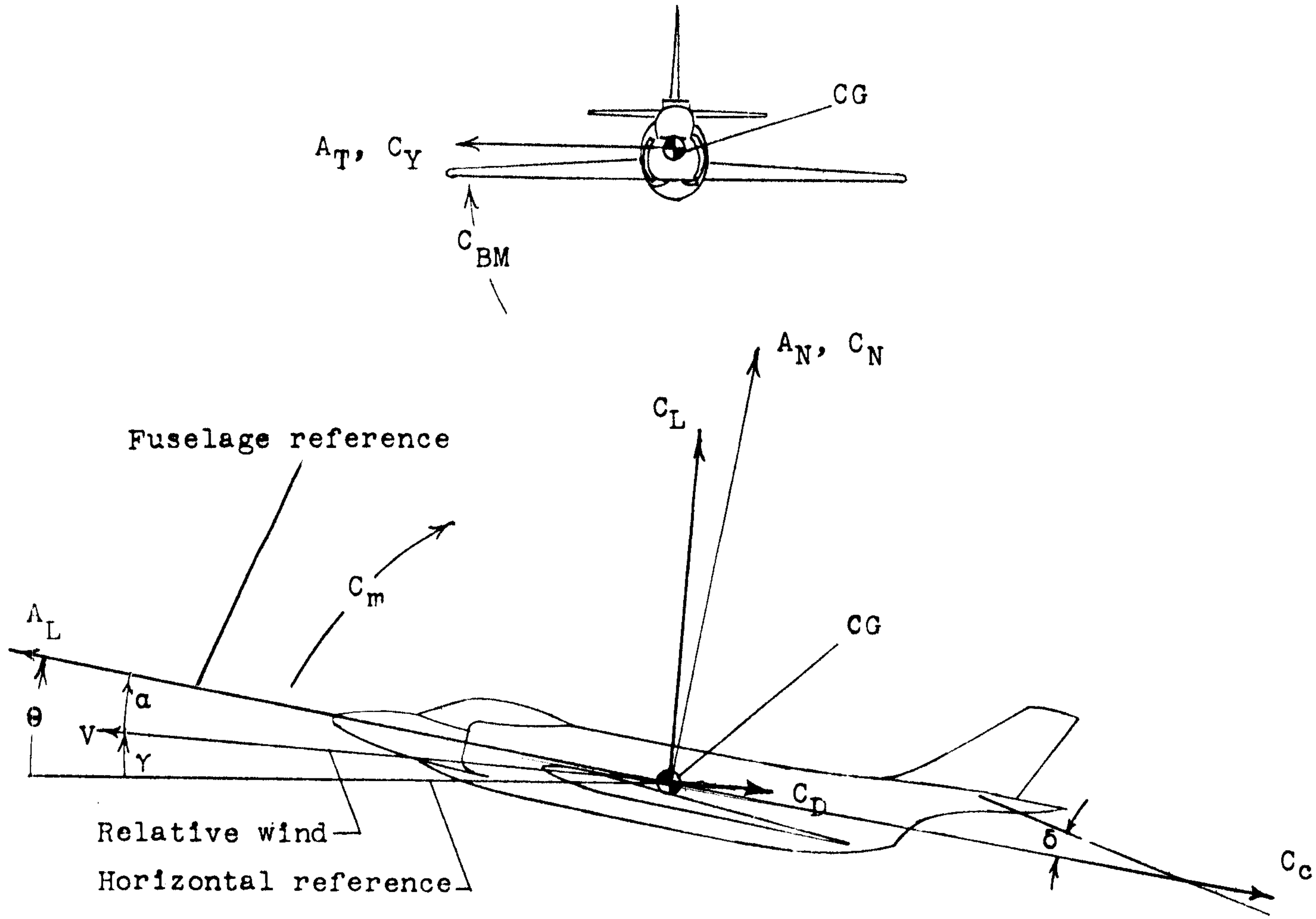

Figure 1.- Positive values of forces, moments, and displacements are indicated by arrows.

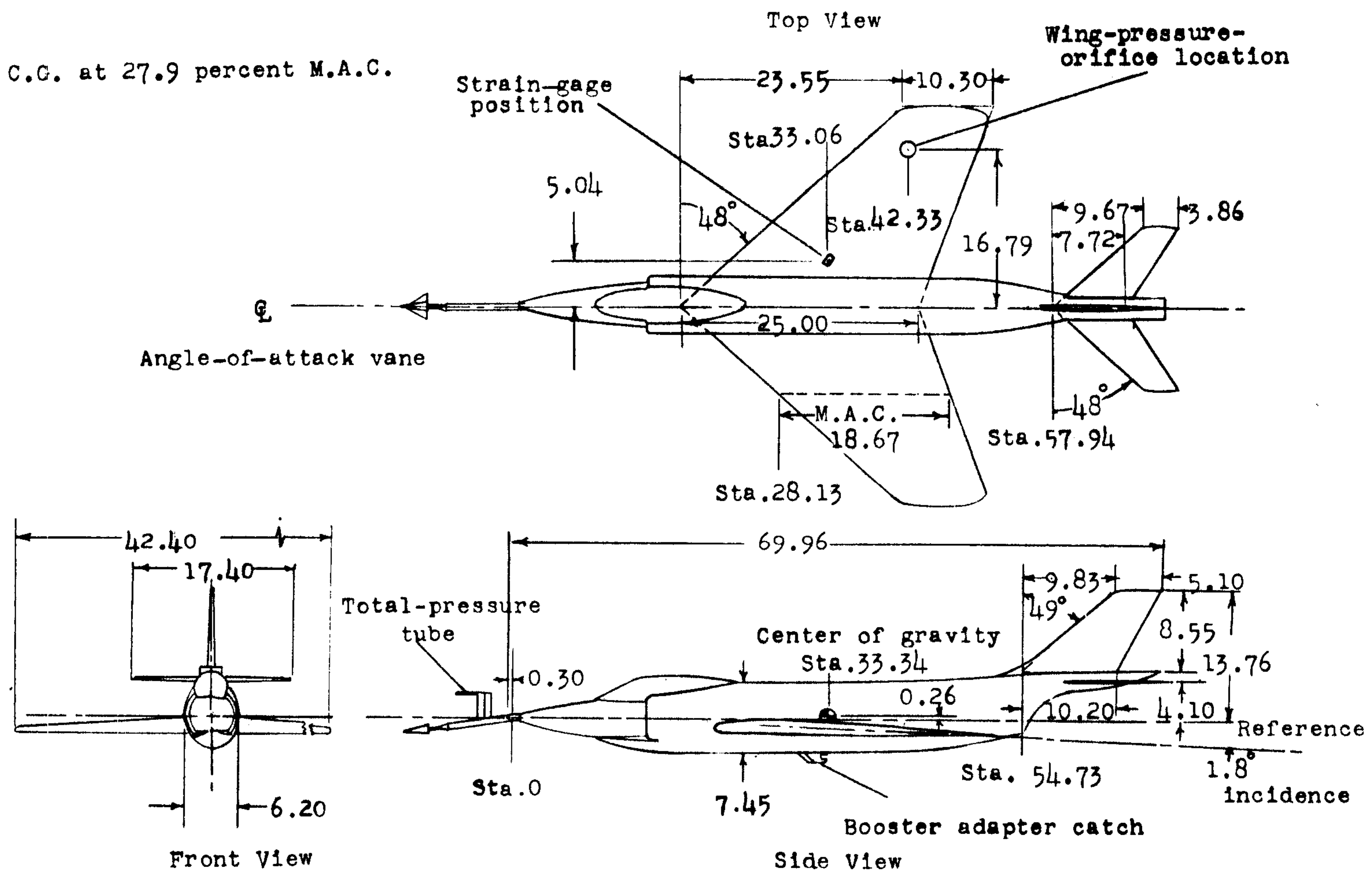

(a) Three-view drawing of the 1/10-scale model of the McDonnell F3H-2N airplane. All dimensions are in inches.

Figure 2.- Model description.

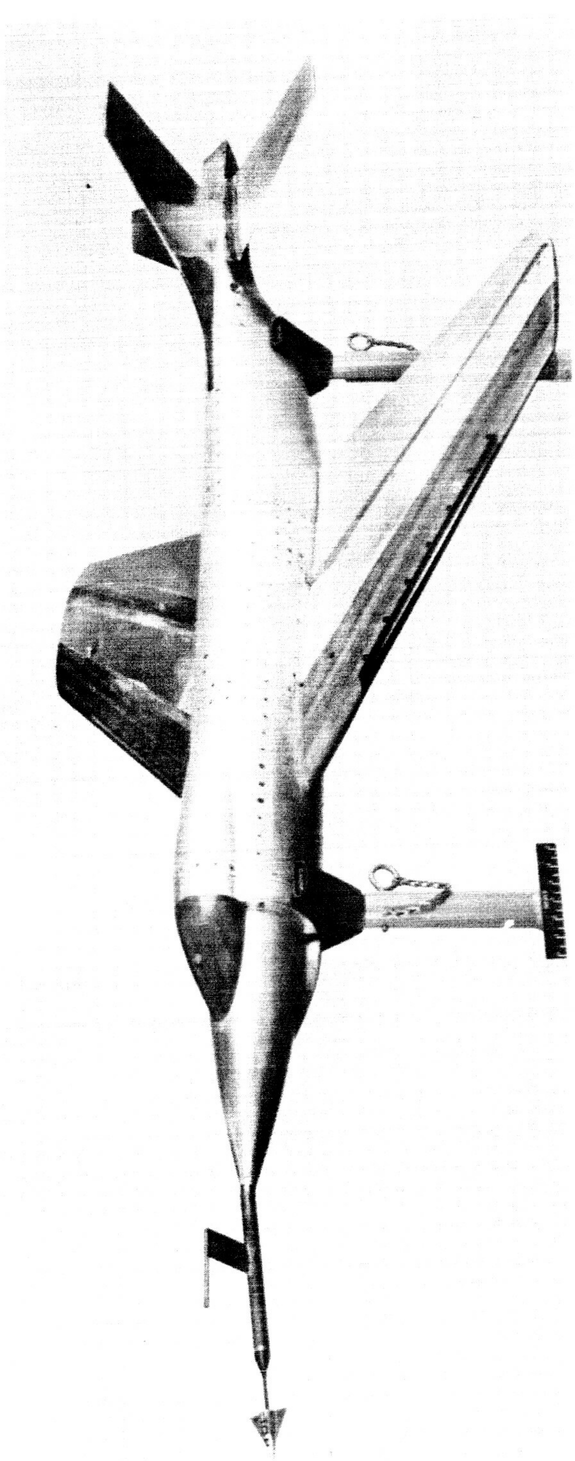

L-89695

(b) Photograph of the model.

Figure 2.- Continued.

Node lines
--X-- indicates node line occurring when
model was continuously shaken at X cycles per second.

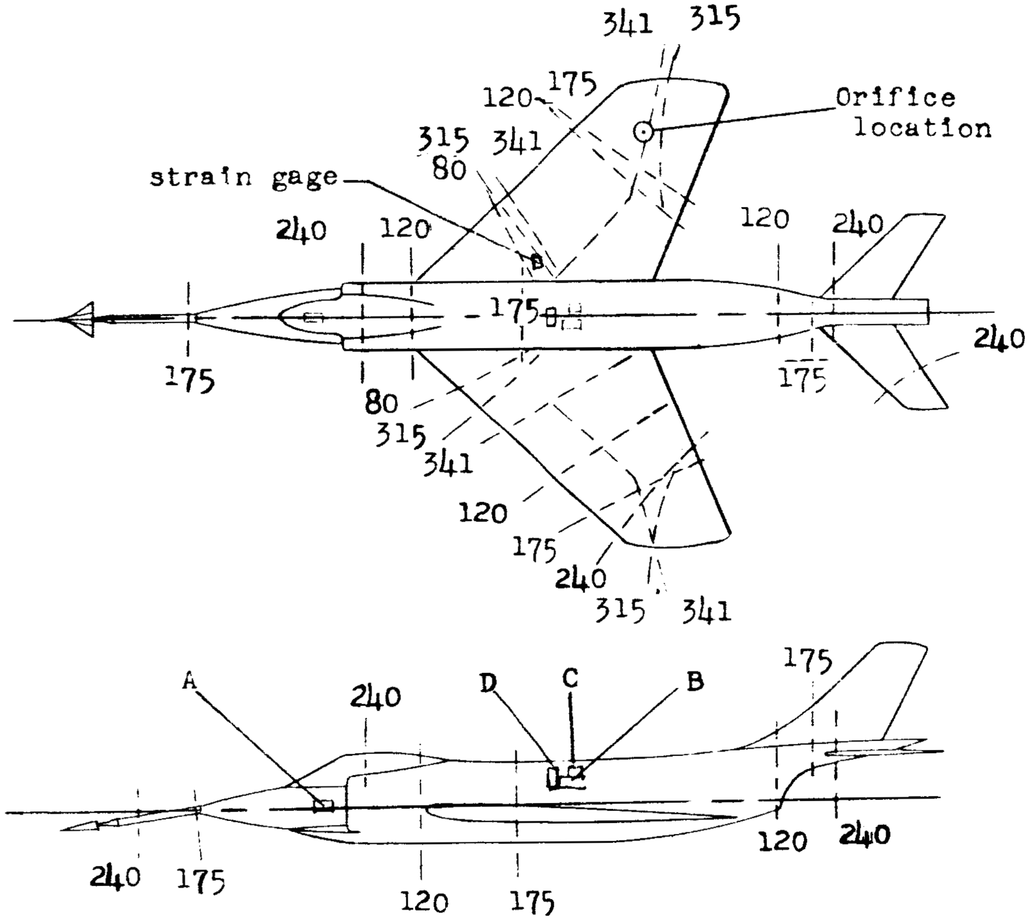

Accelerometer locations
A, normal at nose
B, normal at cg
C, chordwise
D, transverse

(c) Nodal lines and resonant frequencies at which they occurred in the shake test.

Figure 2.- Continued.

[redacted]

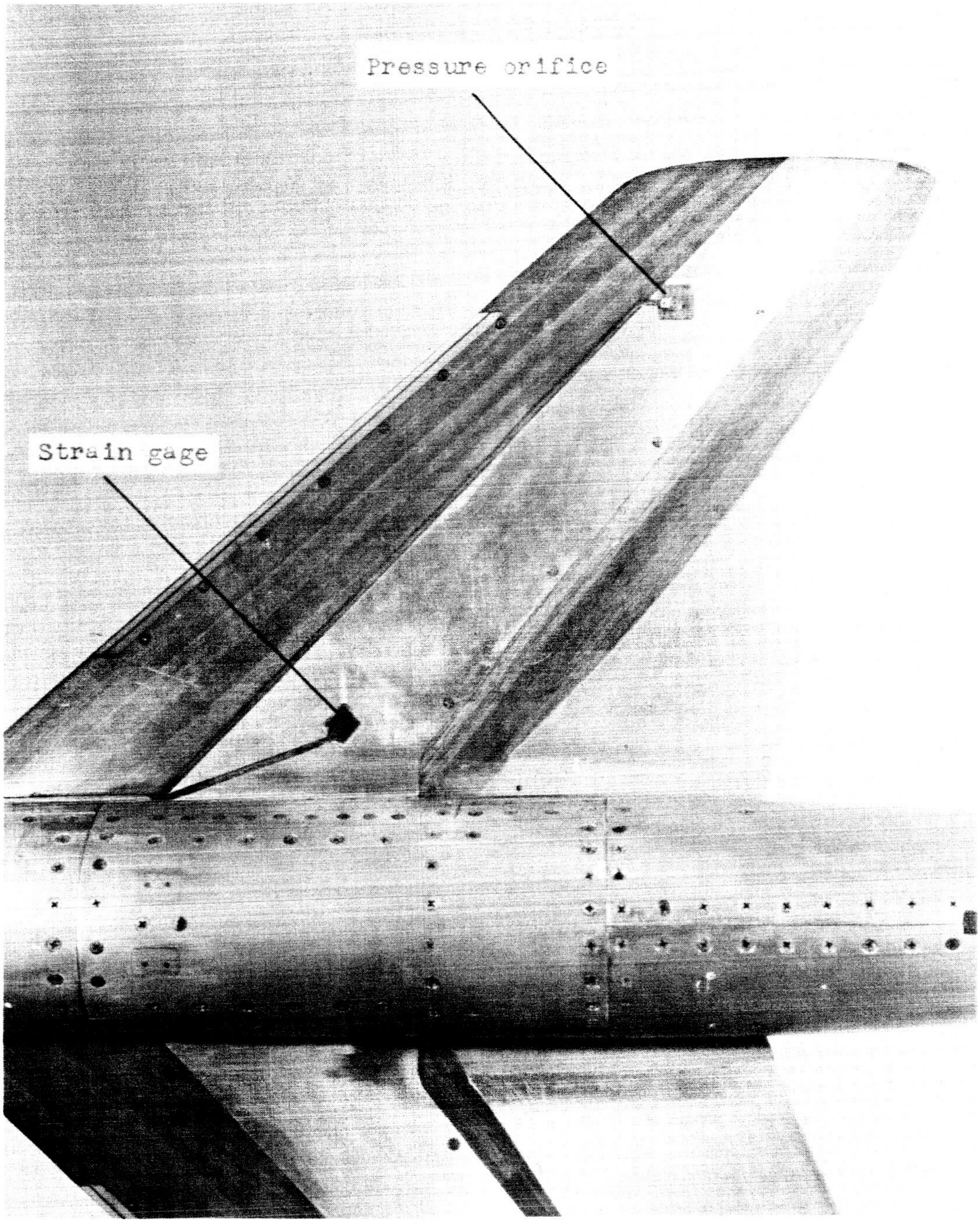

L-89696.1

(d) Photograph of the upper surface of the right wing showing the strain-gage and pressure-orifice installations.

Figure 2.- Concluded.

[redacted]

DECLASSIFIED [redacted]

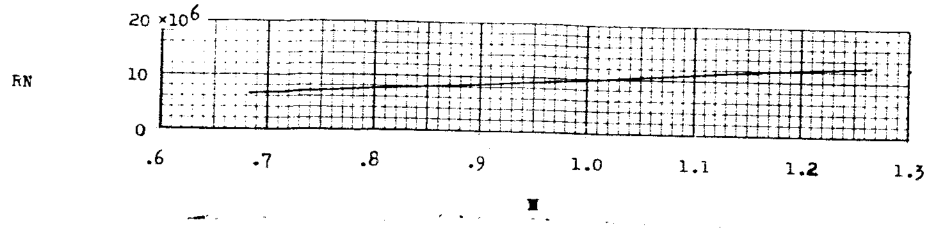

(a) Reynolds number.

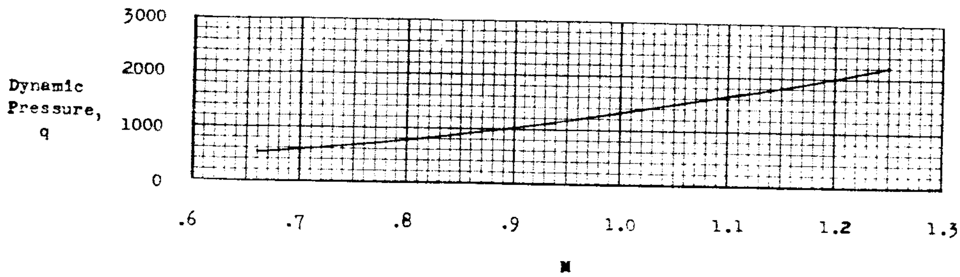

(b) Dynamic pressure.

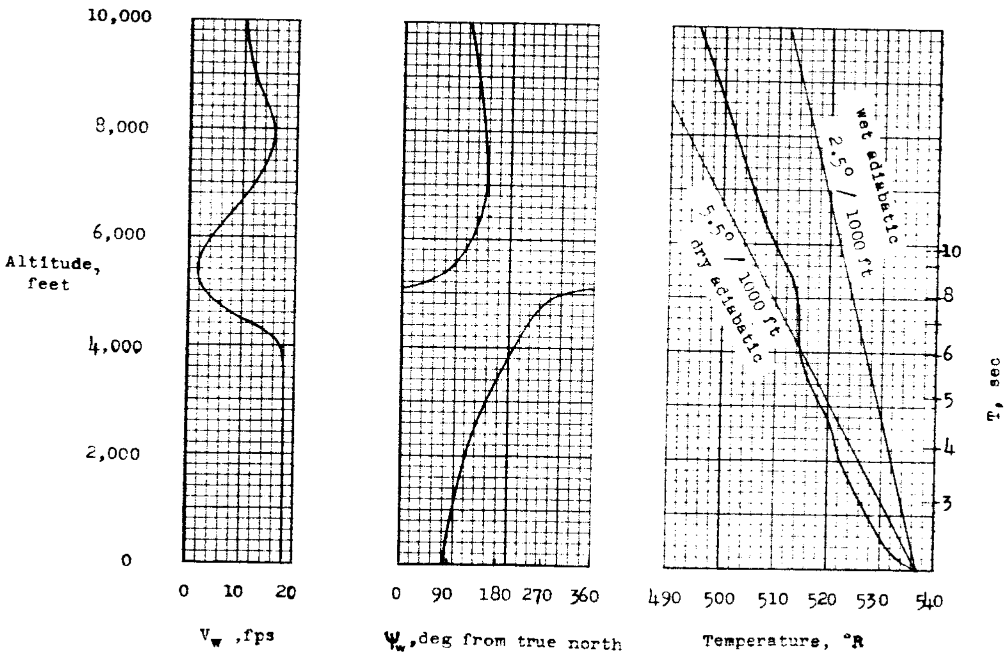

(c) Meteorological conditions at the test site.

Figure 4.- Test conditions.

[redacted]

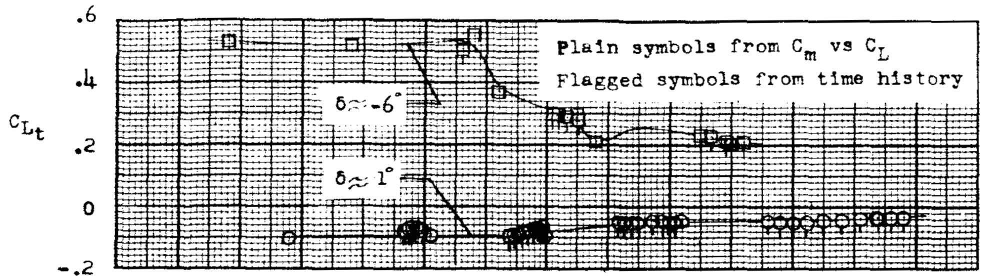

(a) Trim lift coefficient.

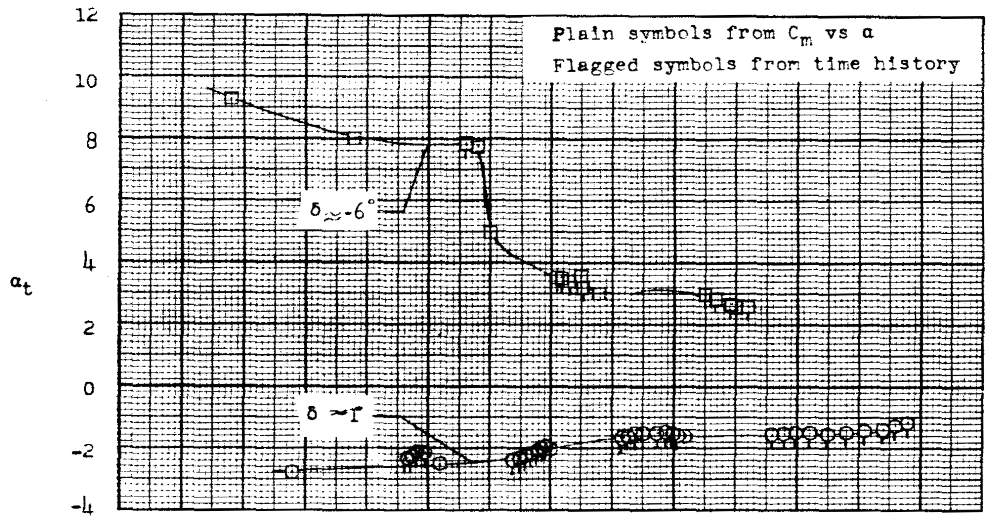

(b) Trim angle of attack of fuselage reference.

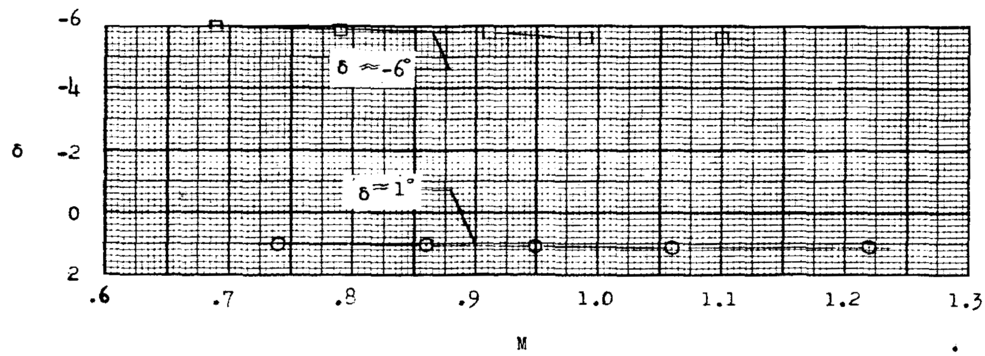

(c) Stabilizer incidence relative to fuselage reference.

Figure 5.- Trim characteristics.

[redacted]

[redacted]

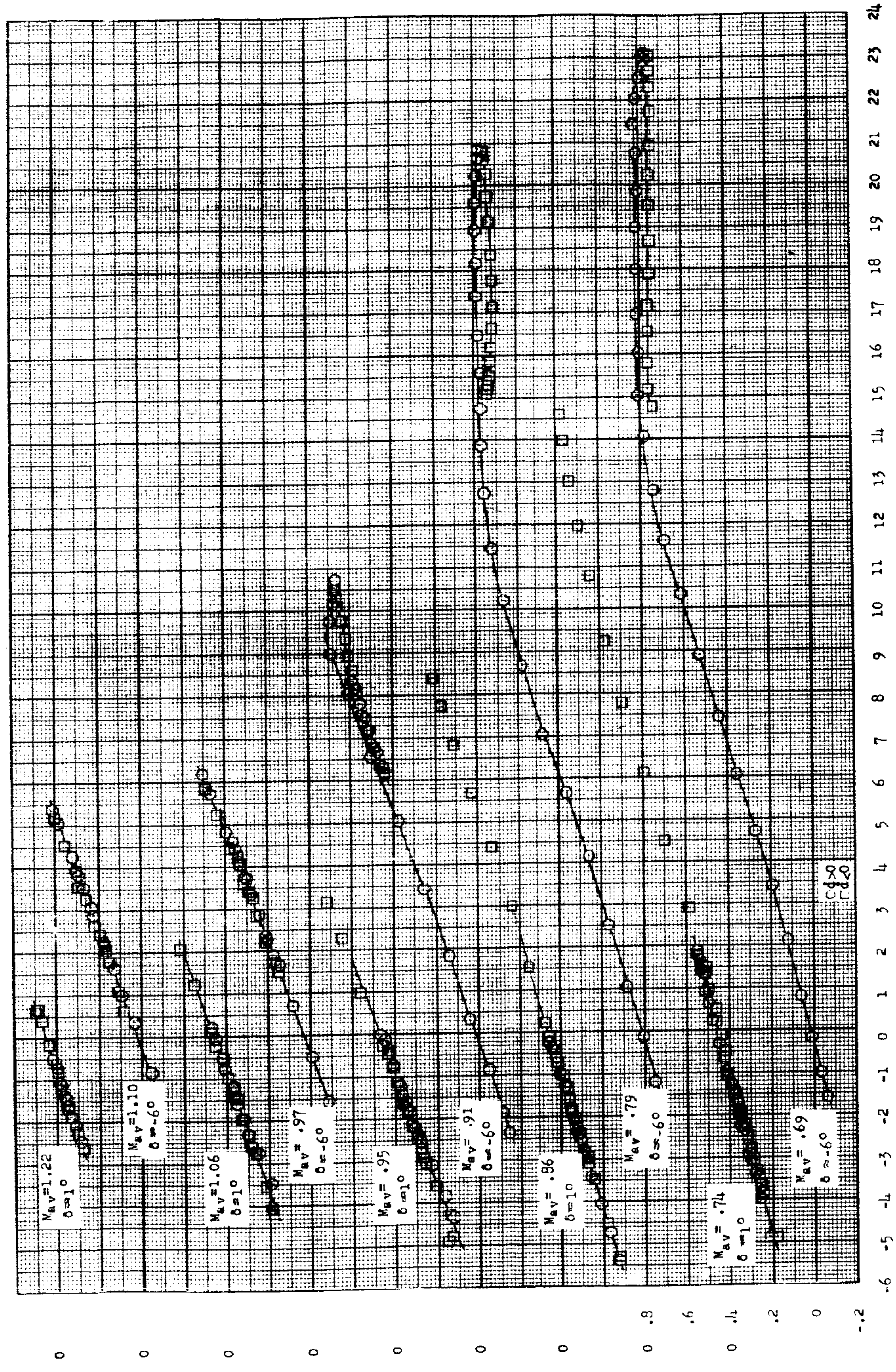

Figure 6.- Basic lift data.

[redacted]

 [redacted]

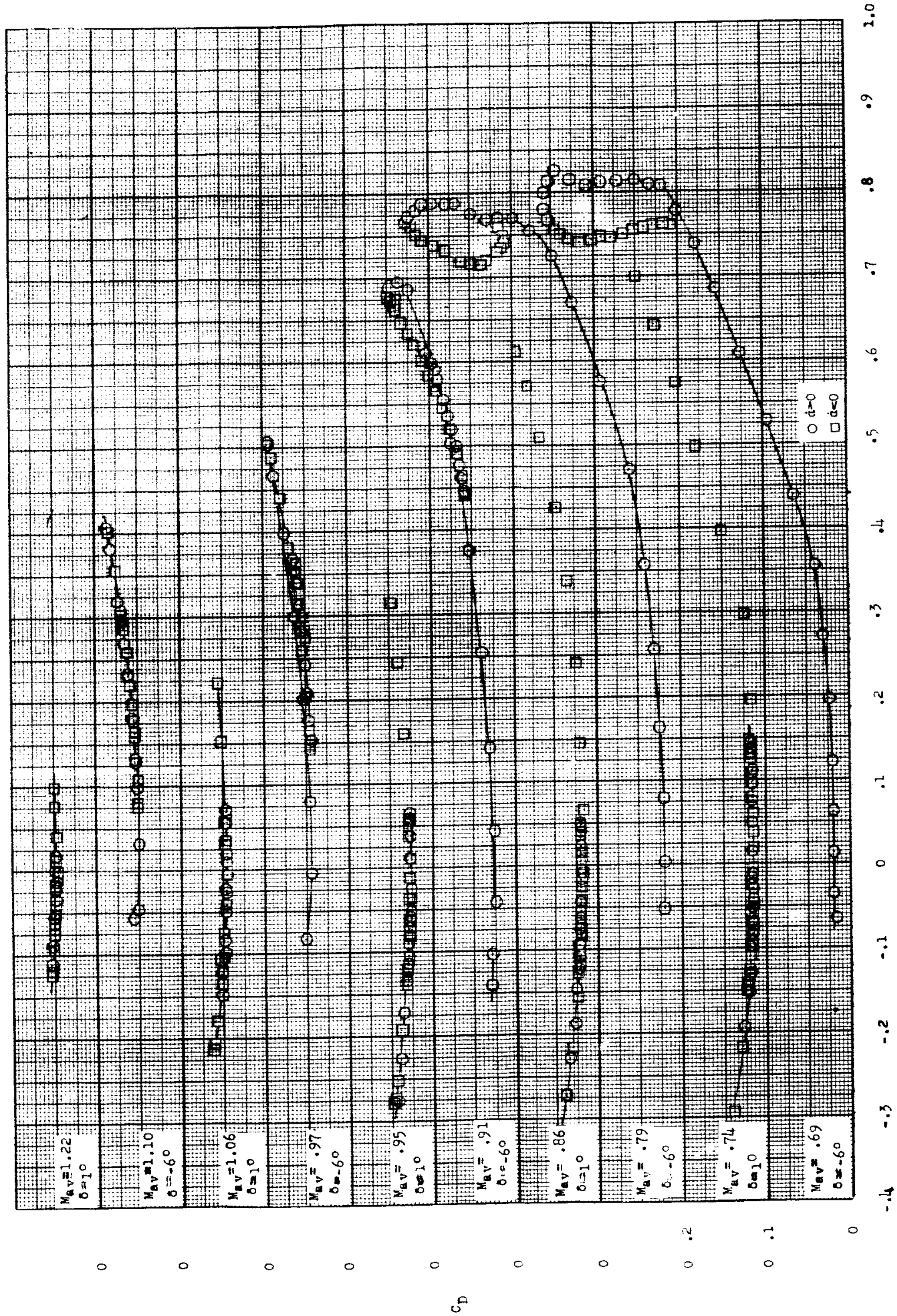

Figure 8.- Basic drag data.

[redacted]

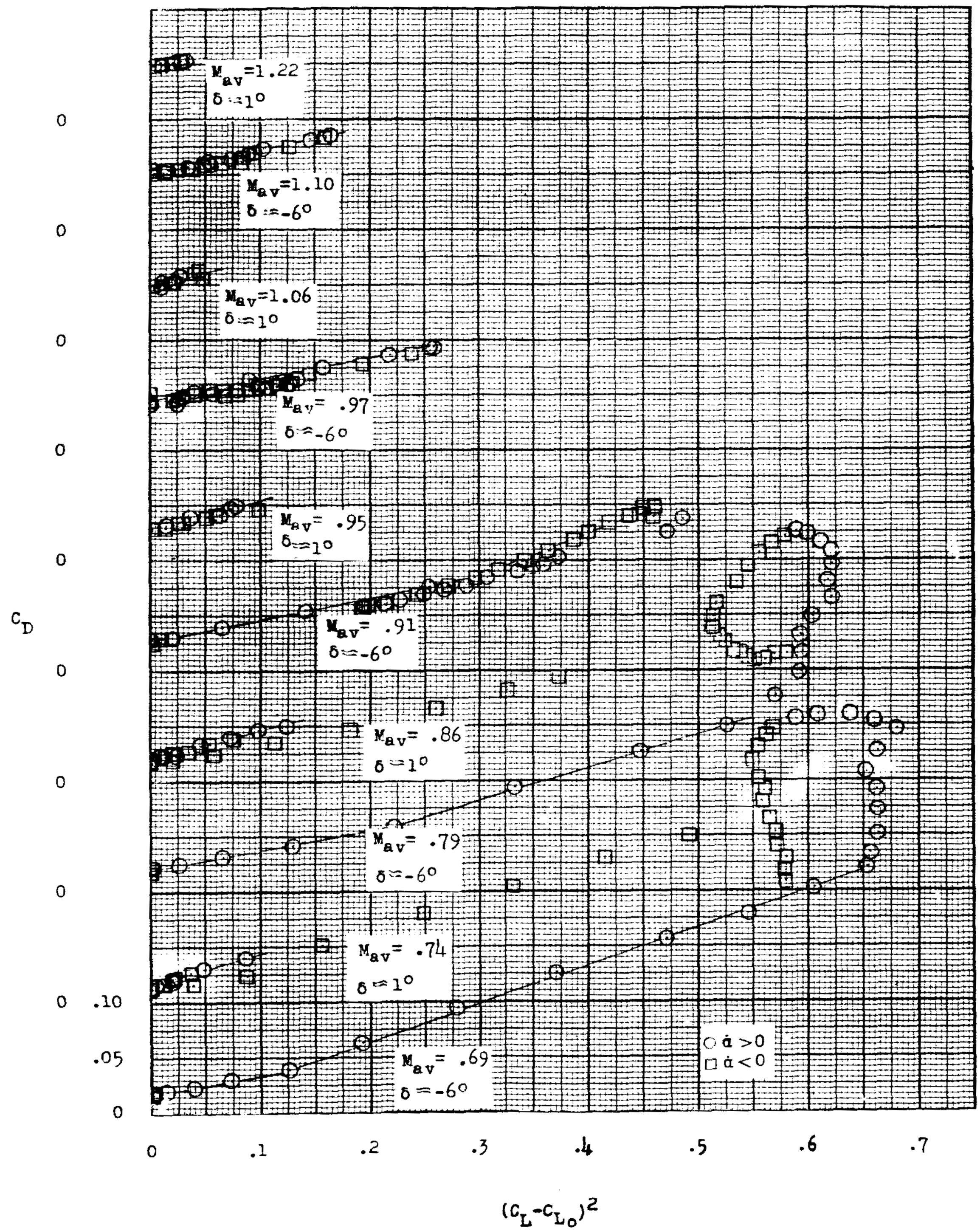

Figure 9.- Induced-drag analysis.

 DECLASSIFIED [redacted]

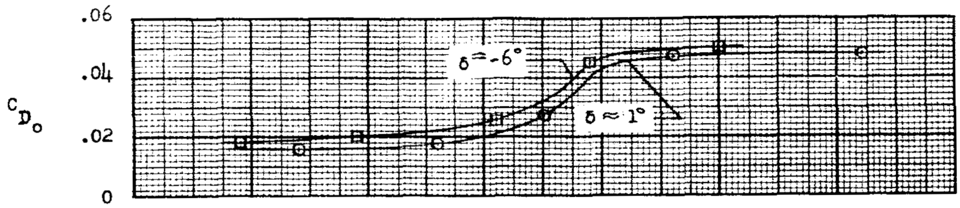

(a) Minimum drag.

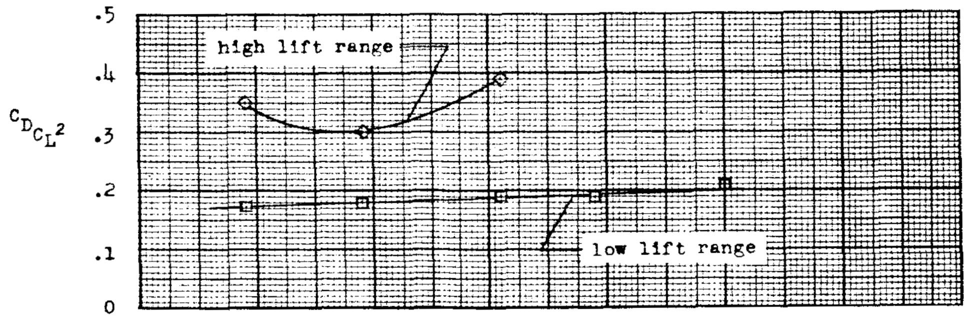

(b) Induced drag.

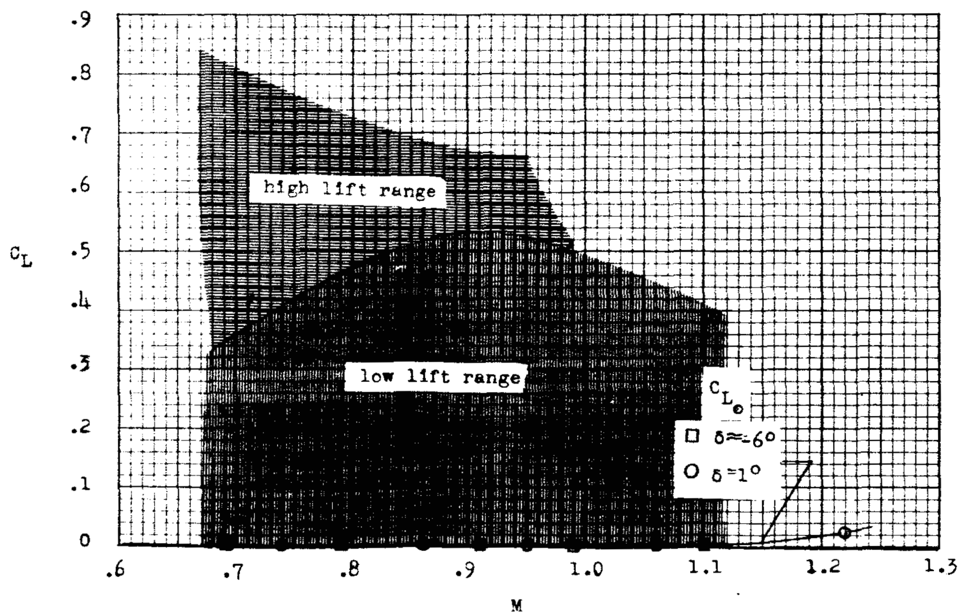

(c) C_L ranges for induced-drag factors.

Figure 10.- Drag summary.

[redacted]

[redacted]

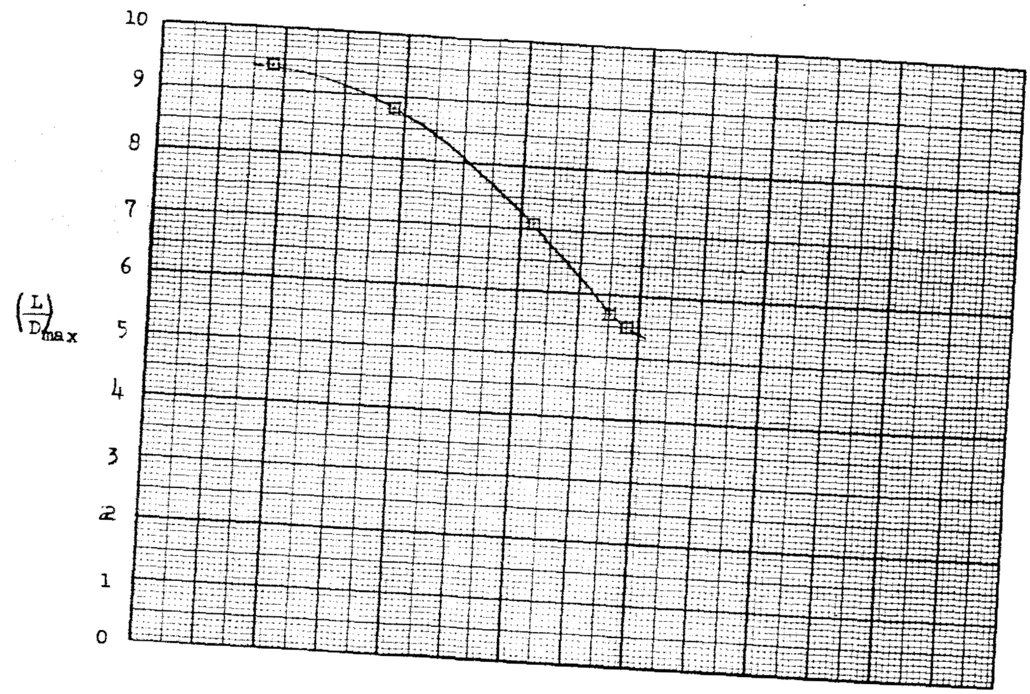

(d) $(L/D)_{max}$; $\delta \approx -6^{\circ}$.

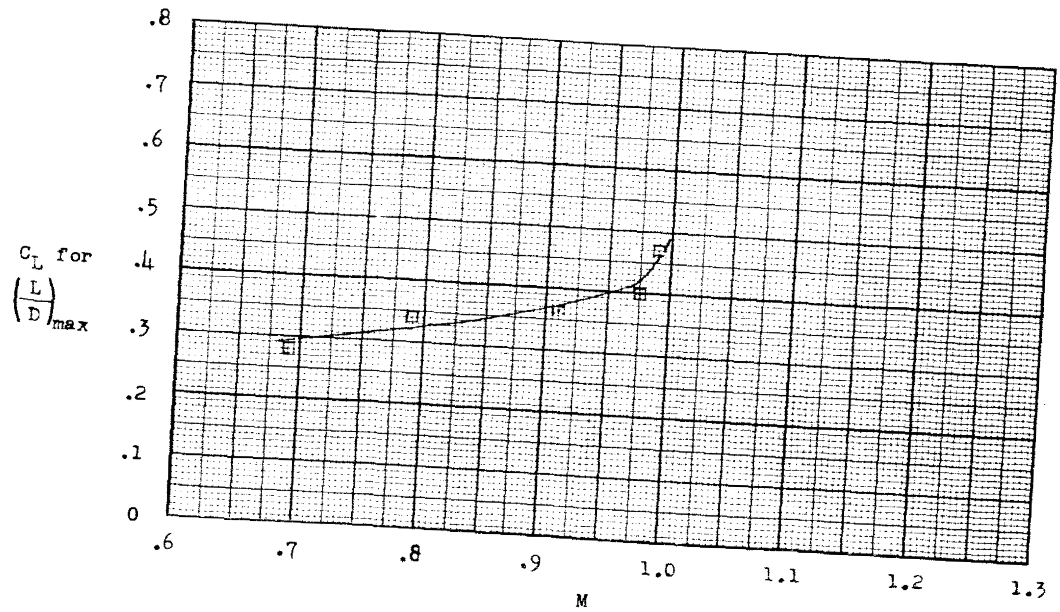

(e) C_L for $(L/D)_{max}$; $\delta \approx -6^{\circ}$.

Figure 10.- Concluded.

[redacted]

DECL[redacted]IED

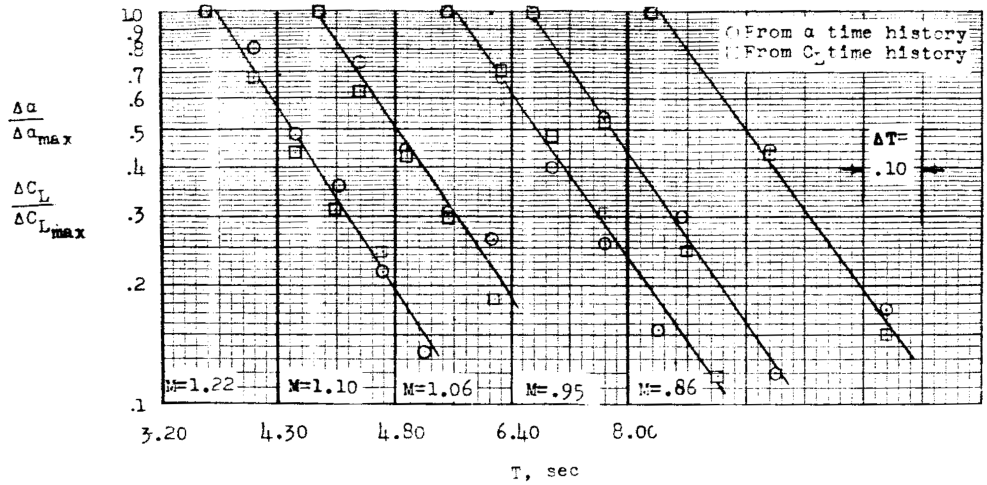

(a) Incremental amplitude ratios plotted against time for C_L and α.

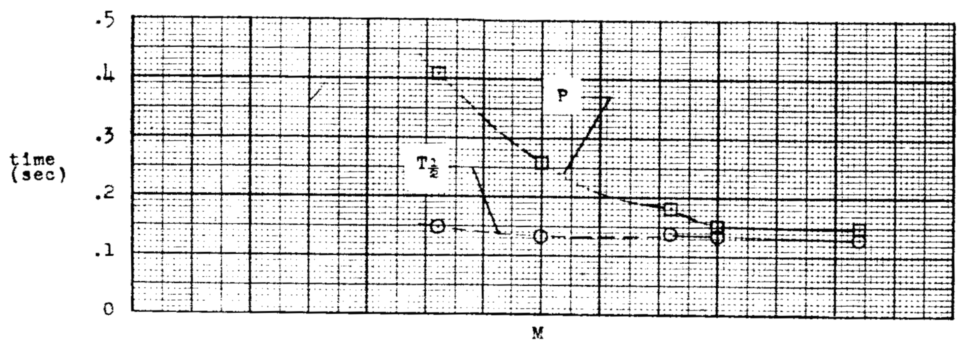

(b) Period and time to damp to half amplitude of the longitudinal oscillations.

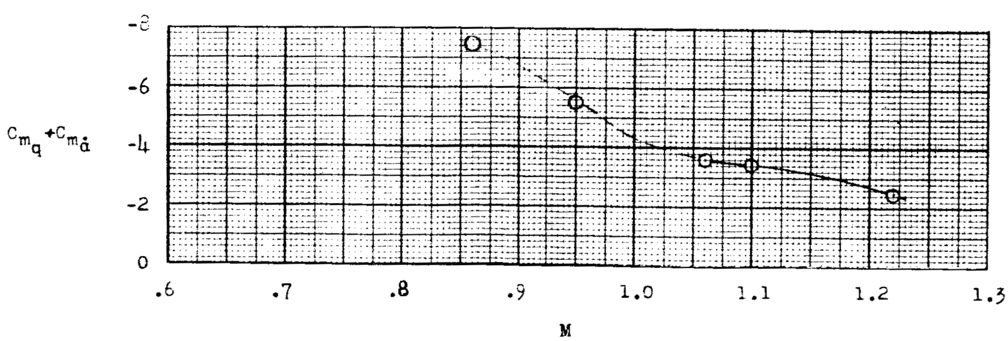

(c) Total damping derivative.

Figure 11.- Dynamic-stability summary.

[redacted]

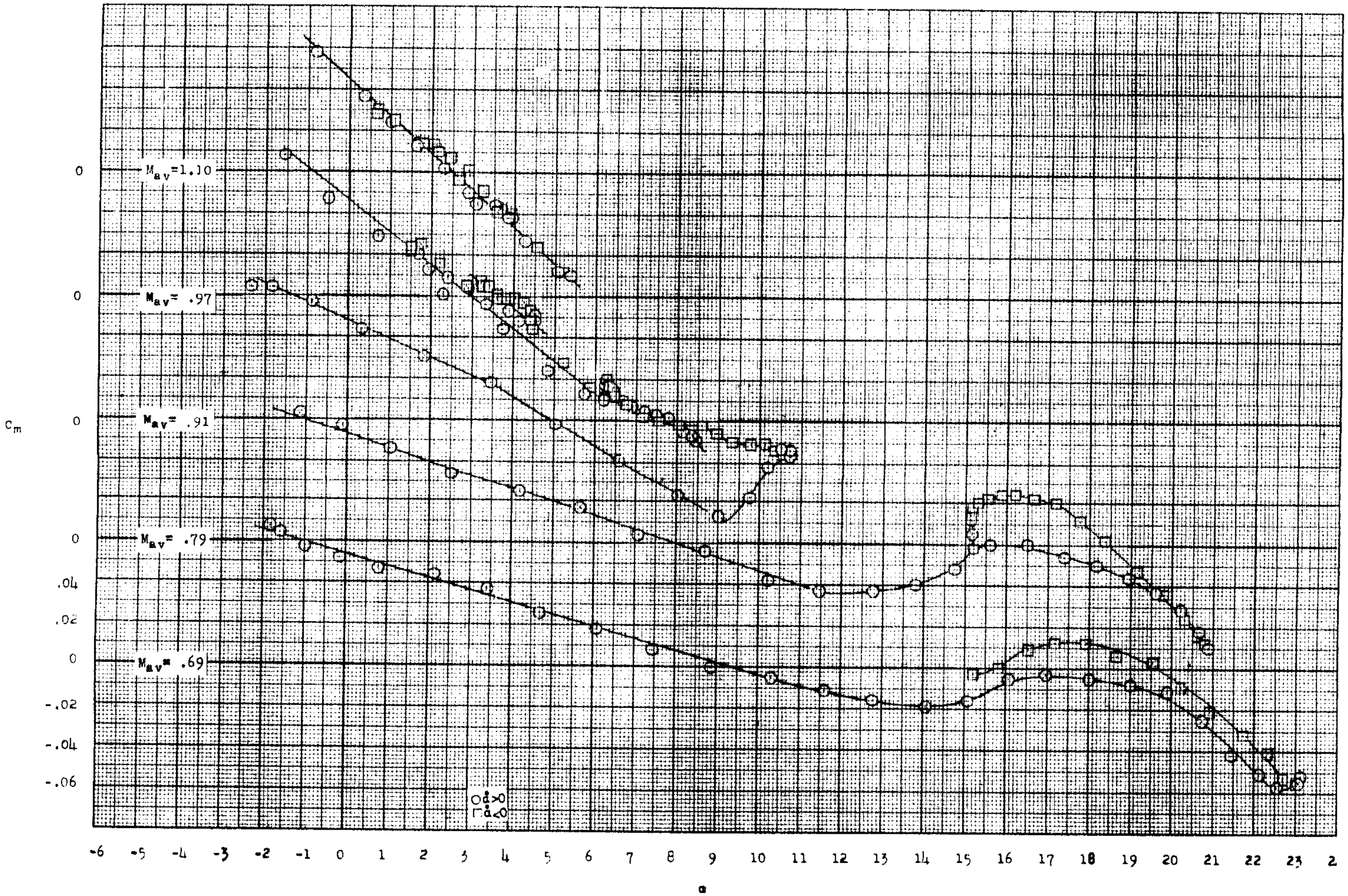

(a) $\delta \approx -6^{\circ}$.

Figure 12.- Basic pitching-moment data, center of gravity at 27.9 percent of mean aerodynamic chord.

[redacted]

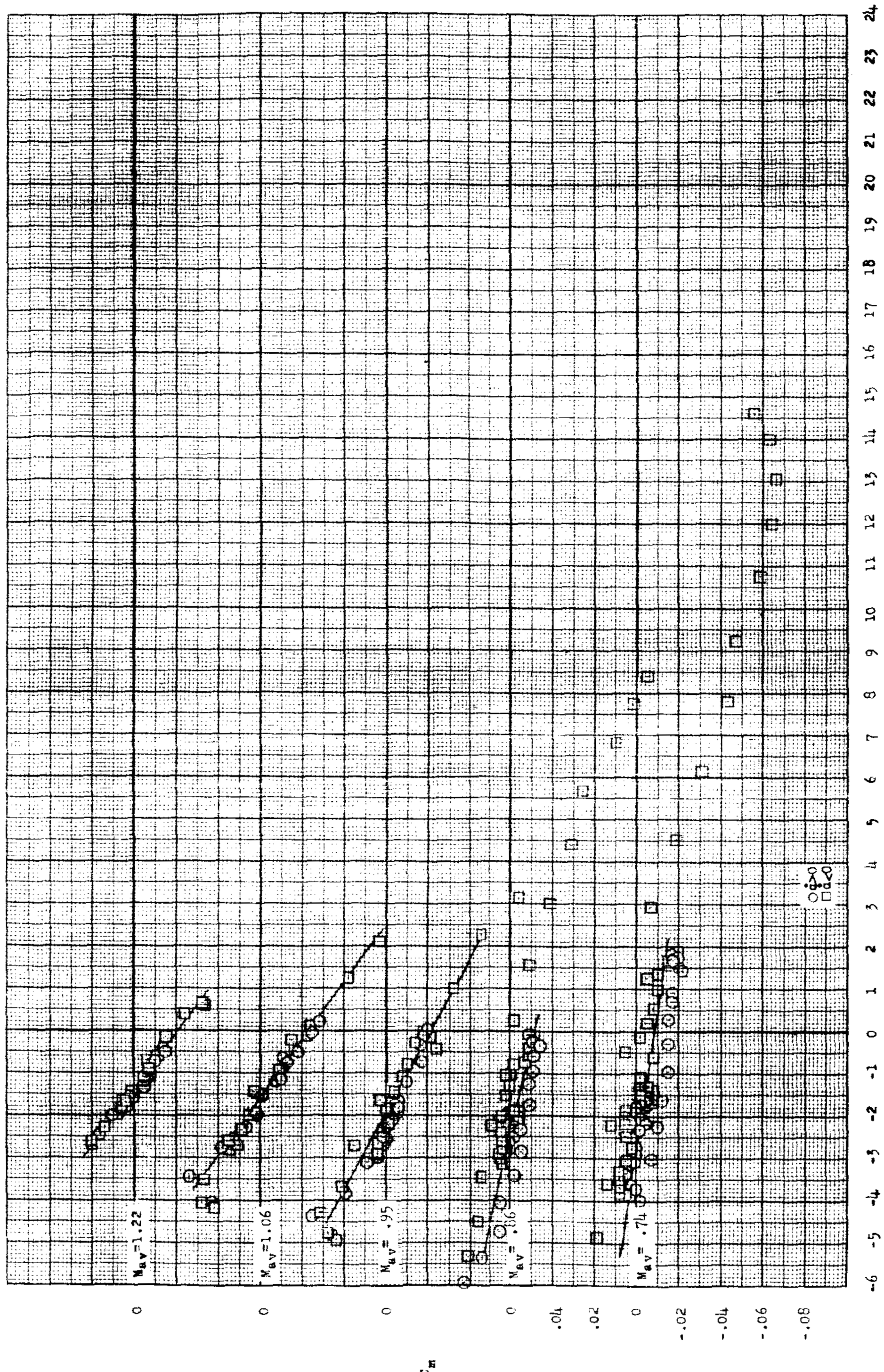

(b) $\delta \approx 1^{\circ}$.

Figure 12.- Concluded.

[redacted]

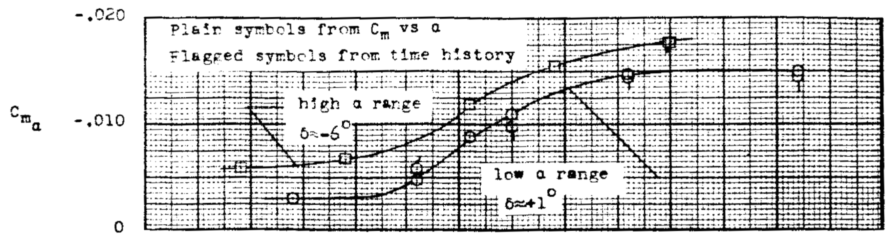

(a) Static stability derivative, center of gravity at 27.9 percent of mean aerodynamic chord.

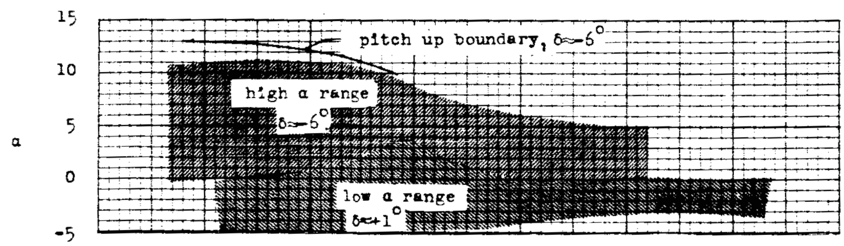

(b) Angle-of-attack ranges for C_{m_α}.

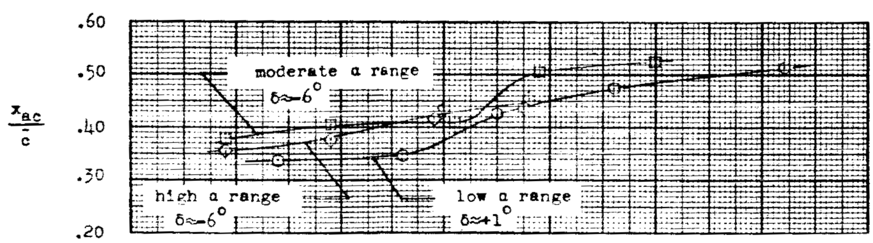

(c) Aerodynamic-center location.

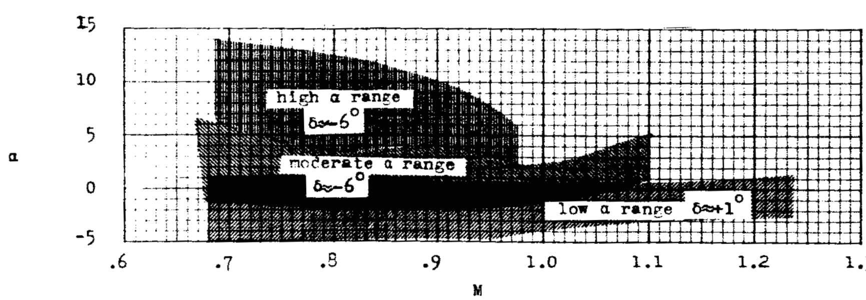

(d) Angle-of-attack ranges for x_{ac}.

Figure 13.- Static-stability summary.

[redacted]

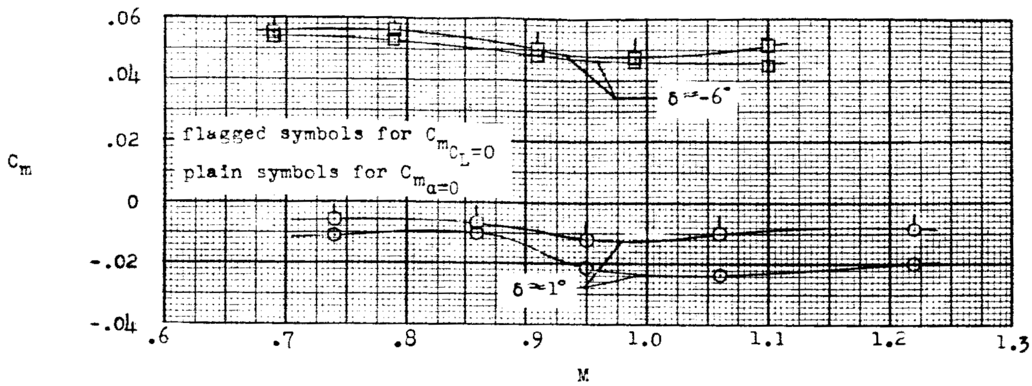

Figure 14.- Out-of-trim pitching-moment coefficient.

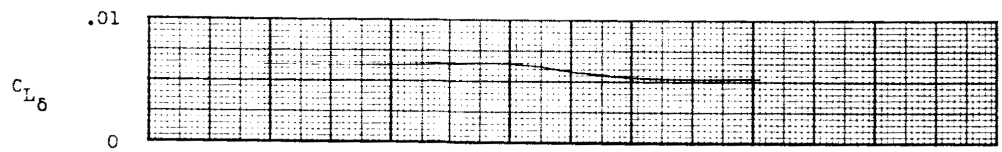

(a) Increment in lift coefficient due to stabilizer deflection.

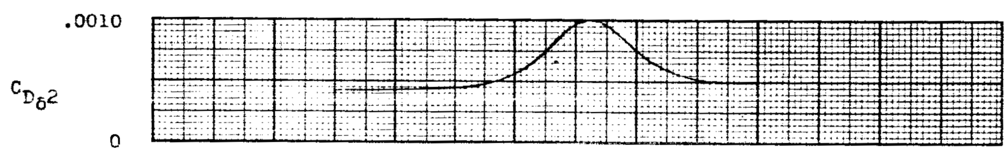

(b) Induced-drag coefficient due to stabilizer deflection.

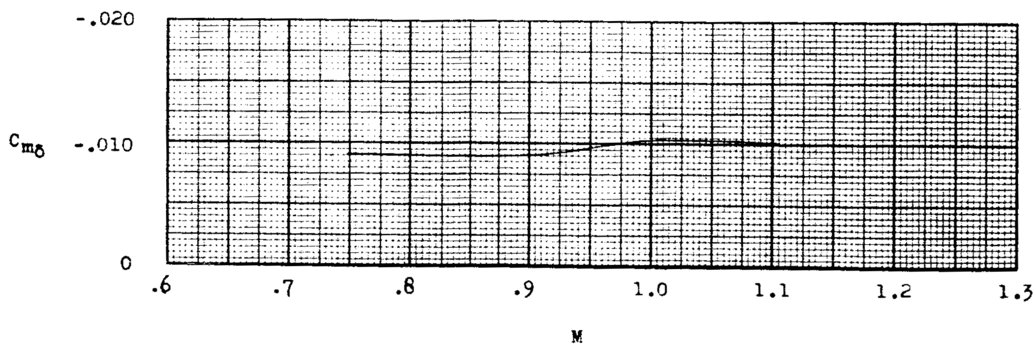

(c) Pitching effectiveness; center of gravity at 27.9 percent of mean aerodynamic chord.

Figure 15.- Stabilizer effectiveness.

[redacted]

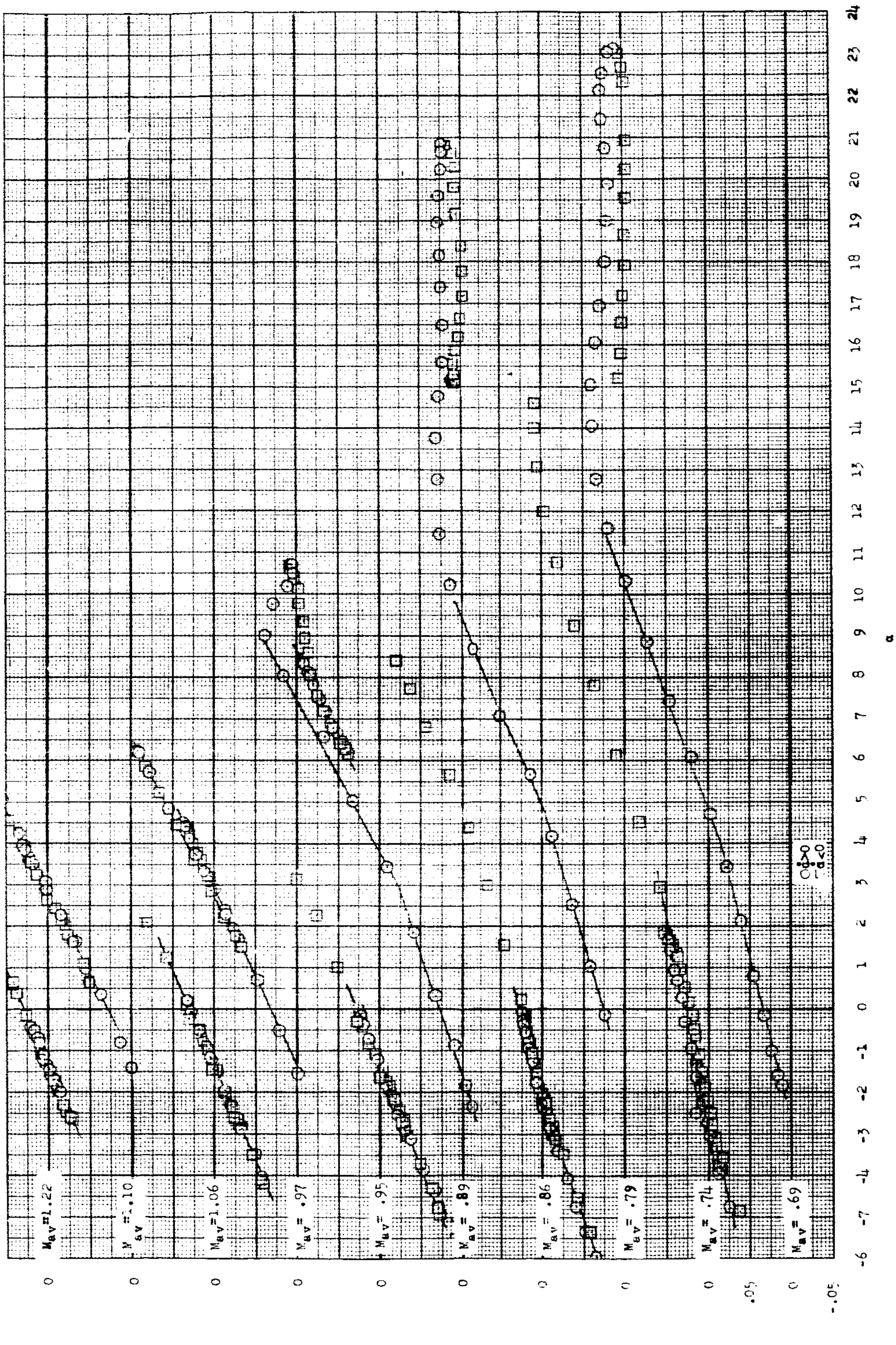

Figure 16.- Basic wing bending-moment data.

[redacted]

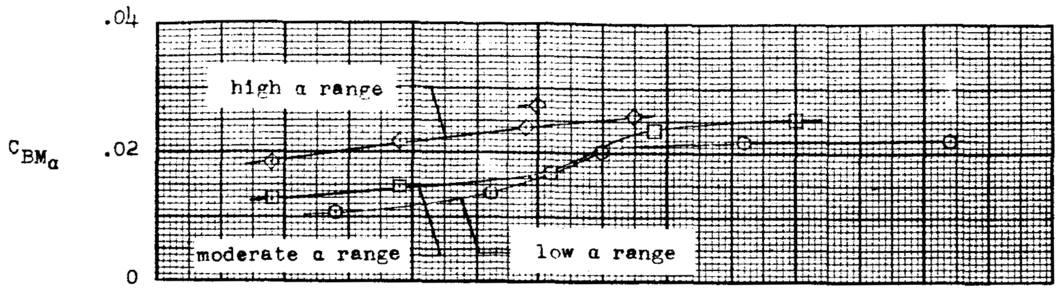

(a) Bending-moment slope.

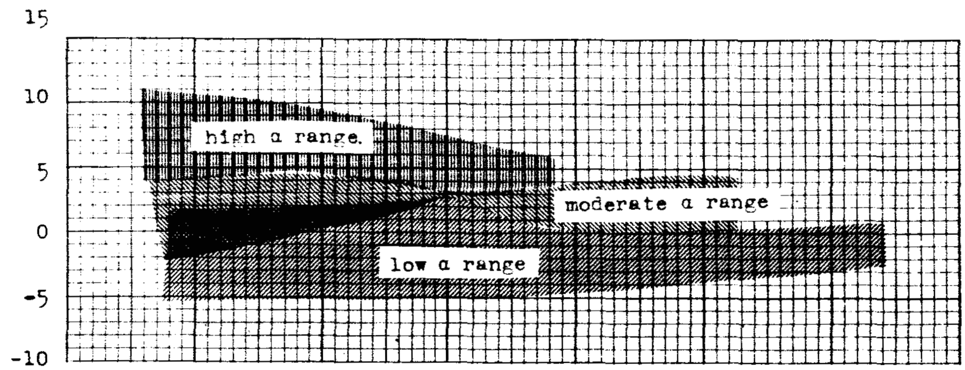

(b) Range of angle of attack for which slopes apply.

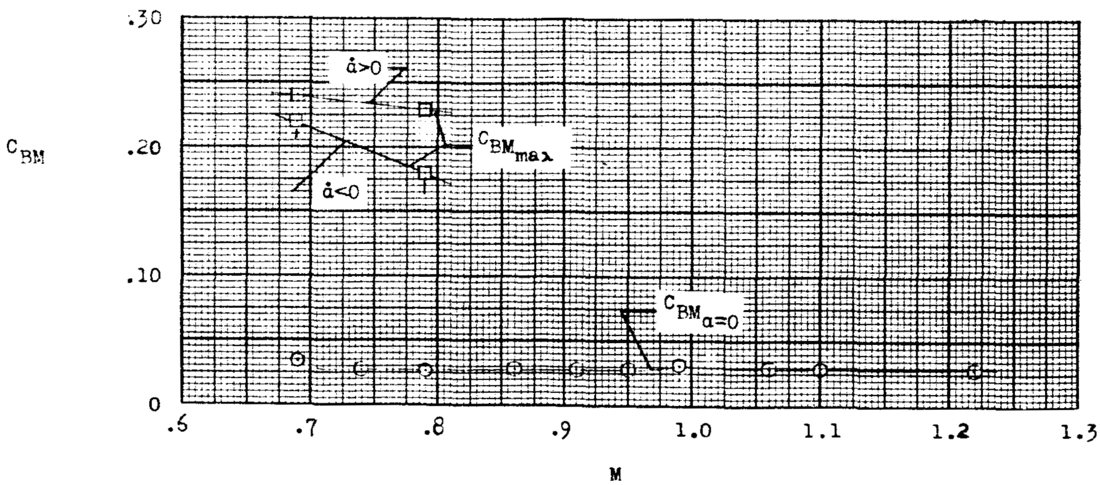

(c) Bending-moment intercept and maximum-bending-moment coefficient.

Figure 17.- Wing bending-moment summary.

[redacted]

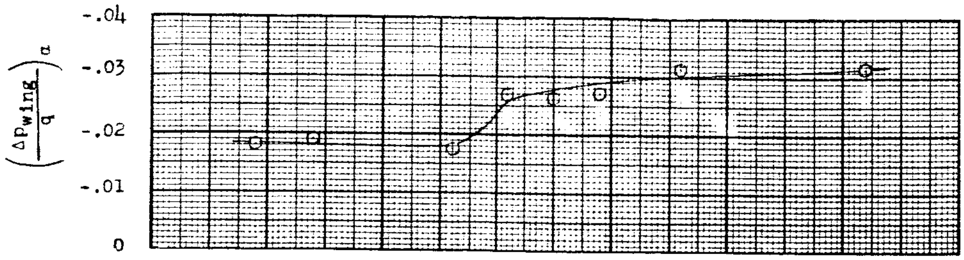

(a) Wing-pressure-coefficient slope.

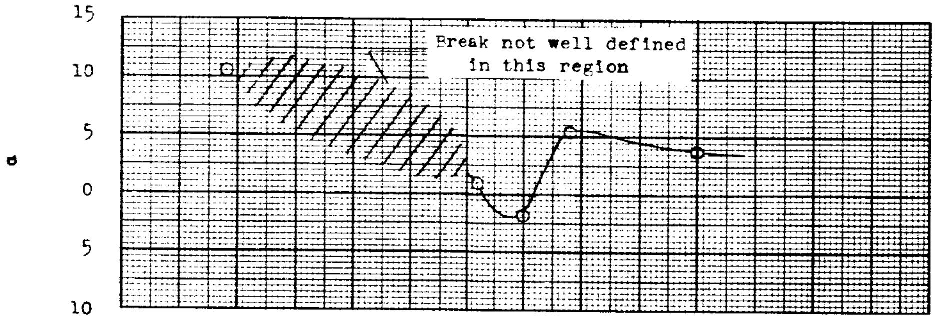

(b) Angle of attack of break in slope.

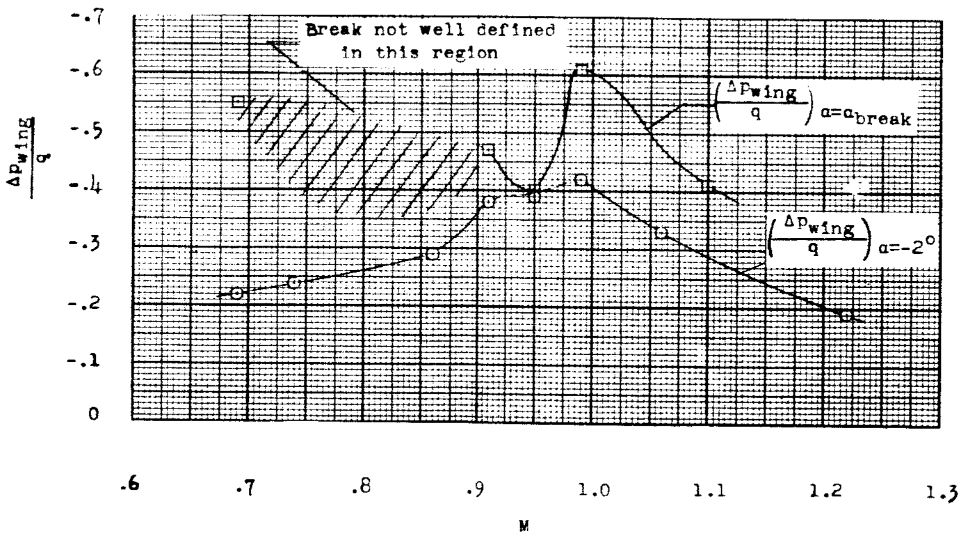

(c) Values of wing pressure coefficient for $\alpha = -2^\circ$ and at break in slope.

Figure 19.- Wing-pressure-coefficient summary.

[redacted]

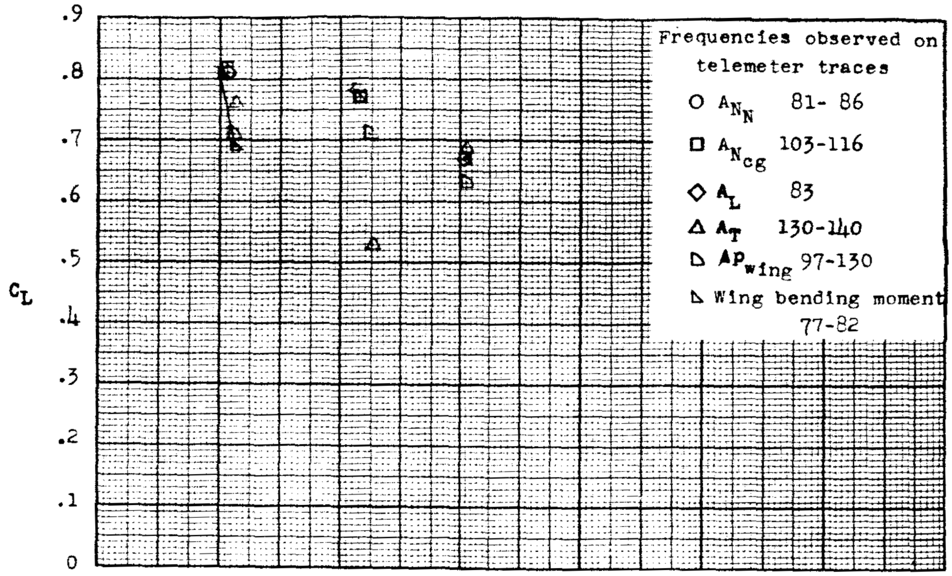

(a) C_L at apparent buffet inception.

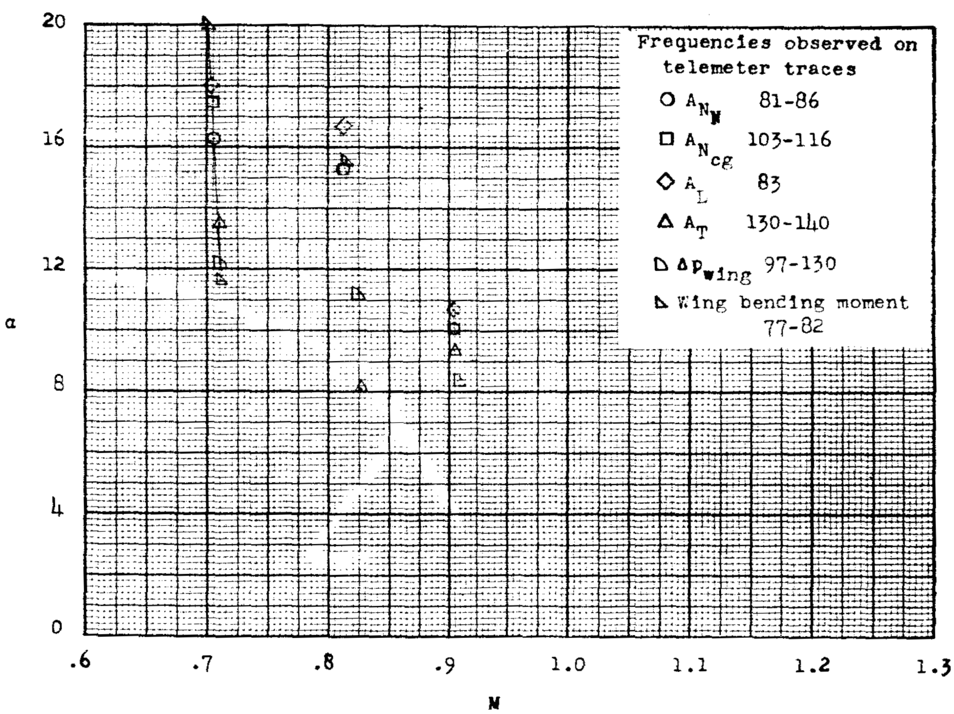

(b) α at apparent buffet inception.

Figure 20.- Buffet summary.

[redacted]

INDEX

Subject	Number
Airplanes - Specific Types	1.7.1.2
Stability, Longitudinal - Static	1.8.1.1.1
Stability, Longitudinal - Dynamic	1.8.1.2.1
Damping Derivatives - Stability	1.8.1.2.3
Control, Longitudinal	1.8.2.1
Stalling	1.8.4
Loads, Aerodynamic - Wings	4.1.1.1

ABSTRACT

A model resembling the McDonnell F3H-2N airplane was tested at transonic speeds by the free-flight technique to determine its pitch-up and buffet boundaries in addition to the longitudinal stability and control data obtainable by the pulse-tail technique.

[redacted]